THE JOURNAL OF BIOLOGICAL CHEMISTRY
Vol. 280, No. 34, Issue of August 26, pp. 30001–30008, 2005
Printed in U.S.A.

Protofibril Formation of Amyloid β-Protein at Low pH via a Non-cooperative Elongation Mechanism*

Received for publication, January 3, 2005, and in revised form, April 29, 2005
Published, JBC Papers in Press, June 28, 2005, DOI 10.1074/jbc.M500052200

Rita Carrotta, Mauro Manno‡, Donatella Bulone, Vincenzo Martorana, and Pier Luigi San Biagio

From the Italian National Research Council, Institute of Biophysics at Palermo, via U. La Malfa 153, I-90146 Palermo, Italy

Deposition of the amyloid β-protein (Aβ) in senile or diffuse plaques is a distinctive feature of Alzheimer's disease. The role of Aβ aggregates in the etiology of the disease is still controversial. The formation of linear aggregates, known as amyloid fibrils, has been proposed as the onset and the cause of pathological deposition. Yet, recent findings suggest that a more crucial role is played by prefibrillar oligomeric assemblies of Aβ that are highly toxic in the extracellular environment. In the present work, the mechanism of protofibril formation is studied at pH 3.1, starting from a solution of oligomeric precursors. By combining static light scattering and photon correlation spectroscopy, the growth of the mass and the size of aggregates are determined at different temperatures. Analysis and scaling of kinetic data reveal that under the studied conditions protofibrils are formed via a single non-cooperative elongation mechanism, not prompted by nucleation. This process is well described as a linear colloidal aggregation due to diffusion and coalescence of growing aggregates. The rate of elongation follows an Arrhenius law with an activation enthalpy of 15 kcal mol^{-1}. Such a value points to a conformational change of peptides or oligomers being involved in binding to protofibrils or in general to a local reorganization of each aggregate. These results contribute to establishing a clearer relation at the molecular level between the fibrillation mechanism and fibrillar precursors. The observation of a non-cooperative aggregation pathway supports the hypothesis that amyloid formation may represent an escape route from a dangerous condition, induced by the presence of toxic oligomeric species.

A clear hallmark of Alzheimer disease is the presence in the brain of extracellular amyloid plaques containing a certain amount of cleavage products of the transmembrane amyloid β-protein precursor (1). These are small peptides of 39–42 residues with a hydrophobic domain at the C terminus. They have been found in the core of senile plaques in typical linear aggregates, known as amyloid fibrils. Similar amyloid fibrils made from different proteins or peptides are associated with other neurodegenerative diseases, such as Parkinson and Huntington diseases, and transmissible spongiform encephalopathy (2). More generally, a large class of proteins is able to assemble into a fibrillar structure under appropriate conditions that typically favor misfolded or partially unfolded conformations (3, 4). These results support the hypothesis that fibril formation may be the onset if not the very cause of such pathologies (the "Amyloid Hypothesis") (5).

In the case of Alzheimer disease, the relation between clinical symptoms and Aβ[1] production is well established (also confirmed by the known genotype-to-phenotype conversion in familial Alzheimer disease and Down syndrome) (6). However, the amount of amyloid deposits is poorly correlated with pathology, which seems to be primarily related to a synaptic dysfunction preceding neuronal degeneration (7, 8). This neurological effect is mainly due to diffusible oligomers of Aβ rather than to mature amyloid fibers (9, 10). Such oligomeric species, also obtained from amyloid deposits (11, 12), have been found to inhibit long term potentiation (9, 13), cause membrane damage (14, 15), alter membrane fluidity (16), and act as pore-forming toxins (17). These findings have changed the current perspective on the role of amyloid fibrils in neurodegenerative diseases to consider fibrils to be a means of removing dangerous toxic oligomeric species rather than an active pathogenic product (18–20).

Also, the mechanism of amyloid formation often involves beaded chain protofibrils made up of spherical oligomers. This has been found for the Aβ(1–40) at both physiological (21–27) and acid pH (28, 29) and for the Aβ(1–42) (30), as well as for other proteins (31–33). It is still an open question whether such protofibrillar aggregates are on-pathway intermediates in the fibrillogenesis process. However, a certain correlation between their reduction in number and the appearance of mature fibrils has been noticed (29).

In the present work, we study the assembly of amyloid aggregates starting from a solution of Aβ(1–40) at pH 3.1 containing a distribution of oligomers. Our central issue concerns the mechanism of aggregation in the early stage of kinetics when oligomers assemble into protofibrils (28), *i.e.* structures observed before or during the formation of mature amyloid fibrils (34). To focus on the details of the assembly mechanism and to develop a reasonable model for protofibril formation, we chose to work at acid pH, a condition that allows easy seed-free preparations and, hence, reproducible kinetics (35, 36). Also, at this pH the overall process occurs on a time scale that is suitable to be studied over a wide range of temperatures (37).

In the human body Aβ assembly occurs in a very complex environment, characterized by a given pH, a low peptide concentration, and the presence of certain amount of different proteins, membranes, metal ions, and other biomolecular objects. *In vitro* experiments are performed on extremely

* This work was partially supported by the Italian Ministero della Salute through the projects "Animal Neuropathies: Molecular and Functional Analyisis of Prion Protein in Sicilian Bovine Species" and "Deposit of Amyloid β-Protein in Cellular Membrane: Role of Metal Ions and Free Radicals." The costs of publication of this article were defrayed in part by the payment of page charges. This article must therefore be hereby marked "*advertisement*" in accordance with 18 U.S.C. Section 1734 solely to indicate this fact.

‡ To whom correspondence should be addressed. Tel.: 39-091-680-9305; Fax: 39-091-680-9349; E-mail: mauro.manno@pa.ibf.cnr.it.

[1] The abbreviations used are: Aβ, amyloid β-protein; QLS, quasielastic light scattering; $\bar{M}_w$, weight average molecular mass.

simplified conditions to highlight a few basic features of the molecular interactions and mechanisms that drive amyloid fibrillogenesis.

At physiological pH Aβ(1–40) forms small oligomers (of a few units) (24–28), whereas, at acid pH (below 3.4), it forms large mass oligomers (with tens of peptides) that readily aggregate into beaded protofibrillar chains (28, 38). It has been proposed that at pH 2, peptides may coexist with spherocylindrical micelles that act as nuclei for fibrillogenesis (35–37, 39).

Our light scattering experiments have shown that the initial oligomers, with an average aggregation number of 75 Aβ(1–40), assemble into elongated linear structures, consistent with previous observations (28) but without any observed nucleation step. Scaling of kinetic data at different temperatures on a single master curve reveals that the same mechanism of aggregation operates between 27 and 67 °C: aggregation proceeds via diffusion and coalescence of clusters and not just by addition of a single monomer to fibrils, as has often been reported under other conditions (35, 36, 40). Also, a single activation free energy barrier has been found to be responsible for the coagulation rate. Interestingly, these experiments go beyond the classic scheme of protein polymerization (41, 42) or amyloid formation (43, 44), which prescribes an elongation process preceded by a rate-limiting nucleation (35, 36, 45–47). In the present work, amyloid formation occurs via a non-cooperative coagulation process, which closely resembles linear colloidal aggregation (33).

EXPERIMENTAL PROCEDURES

Preparation of Peptide Solutions—Samples of 1 mg of Aβ(1–40) powder (purchased from Anaspec, Inc.) were dissolved in 0.2 ml of trifluoroacetic acid and gently stirred at 5 °C for 3 h to completely dissolve associated peptides (48, 49). Upon addition of 1.8 ml of Millipore SuperQ water, solutions were fractionated into five equal parts and lyophilized overnight. This procedure provided stock powder aliquots of the same amount (200 μg). Each aliquot was dissolved in 250 μl of 0.1 M sodium citrate buffer at pH 3.1 and filtered (via a 0.2-μm Millipore filter) into 1-cm square quartz cuvettes or 1-mm cylindrical capillaries. Different peptide concentrations were obtained by diluting the stock powder aliquots by a different amount of buffer solution. All chemicals were reagent grade.

Verification of Seed-free Condition—Pretreatment with trifluoroacetic acid and filtering ensured that no large aggregates (seeds) were present in solution (49). This was readily verified at the beginning of each experiment by quasielastic light scattering measurements, which are very sensitive to high molecular weight objects. The high reproducibility of our kinetics further confirmed the absence of a significant amount of spurious nucleation centers within our peptide solutions, before and after filtering.

Concentration Determination—Concentration was determined by measuring tyrosine absorbance at 276 nm (extinction coefficient: 1390 $cm^{-1}\,M^{-1}$) with a Jasco J-530 spectrometer (50). Peptide concentrations were 185 μM for the main set of experiments. Considering that the molecular mass of Aβ(1–40) is 4.3 kDa, the final concentrations were consistent with those calculated assuming the initial nominal peptide amount of 1 mg, in purchased vials. This confirmed that no material was lost through filtering and that peptide was efficiently dissolved via the trifluoroacetic acid treatment.

Quasielastic Light Scattering—Time-resolved light scattering experiments were performed at different temperatures, immediately after sample dissolution in buffer at pH 3.1. Samples were placed in a thermostatted cell compartment of a Brookhaven Instruments BI200-SM goniometer, equipped with a 100-milliwatt argon laser tuned at $\lambda_0 = 514.5$ nm. The temperature was controlled within 0.05 °C with a thermostatted recirculating bath. Scattered light intensity at 90° and its time autocorrelation function, $g_2(t)$, were measured simultaneously by using a Brookhaven BI-9000 correlator. Correlation functions $g_2(t)$ were analyzed using a constrained regularization method (51) to determine the distribution $P(D)$ of the apparent diffusion coefficients D: $g_2(t) = 1 + |\int P(D)\exp(-Dq^2t)dD|^2$, where q is the scattering vector, defined just below. The z-average hydrodynamic radius R_h was calculated by taking the z-average diffusion coefficient D_z and assuming the Stokes-Einstein relation: $k_BTD_z^{-1} = 6\pi\eta R_h$, where k_B is the Boltzmann constant, T is the temperature, and η is the solvent viscosity (52).

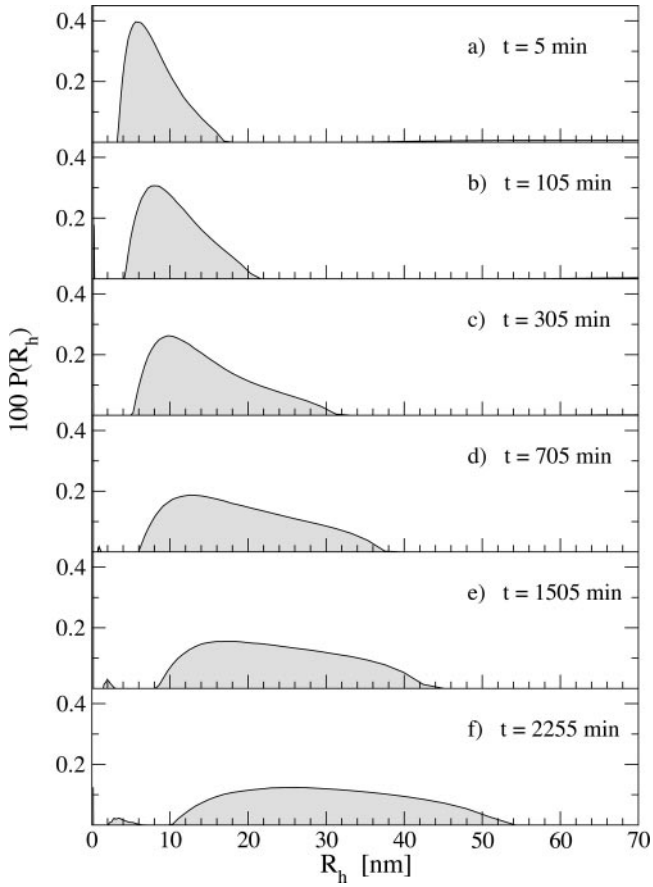

FIG. 1. **Time evolution of the distribution of hydrodynamic radii at 37 °C and 185 μM peptide concentration.** Analysis of QLS data were performed as reported in the text. The distribution is reported in terms of hydrodynamic radii by assuming the Stokes-Einstein relation.

Multiple Angle Light Scattering—The experimental set-up described for QLS experiments was also used for static light scattering measurements. Multiple angle experiments were performed to determine the scattered intensity $I(q)$ at different scattering vectors $q = 4\pi n\lambda_0^{-1}\sin(\vartheta/2)$, where ϑ is the scattering angle and n is the medium refractive index (52). Absolute values for the scattered intensity (Rayleigh ratios) were obtained by normalization with respect to toluene, whose Rayleigh ratio at 514.5 nm was taken as 32×10^{-6} cm^{-1}.

Optical Microscopy—At the end of the scattering experiments, a few drops of solution were put on a glass slide for imaging with a phase-contrast Zeiss Axioskop2 plus microscope.

RESULTS

Onset of Kinetics: Mass and Size of Oligomers—Peptides were dissolved into pH 3.1 buffer to obtain the final concentration of 185 μM. After dissolution, QLS measurements reveal the presence of small size oligomers in the solution, along with a negligible amount of large size aggregates (more than hundreds of nanometers). Apart from this, the distribution of hydrodynamic radii is unimodal with a mean value of $R_h = 7$ nm and a total range 4–15 nm (Fig. 1*a*). Measurement of the intensity scattered at 90° (scattering vector $q = 23$ μm^{-1}) provides the Rayleigh ratio $I_R(q)$ that is related to the weight average molecular mass ($\bar{M}_w$) by the relation: $I_R(q) = 4\pi^2n^2(dn/dc)^2\lambda_0^{-4}N_A^{-1}c\bar{M}_wP_z(q)$, with c the mass concentration, N_A Avogadro's number, and $P_z(q)$ the z-averaged form factor (52). By taking $dn/dc = 0.18$ cm^3g^{-1}, and $P_z(q) = 1$ (because the initial size of oligomers is much smaller than q^{-1}), we obtain a weight average molecular mass $\bar{M}_w = 330 \pm 60$ kDa. Considering that the molecular mass of a single Aβ(1–40) is 4.3 kDa, the soluble oligomers found at the onset of kinetics are made up on average

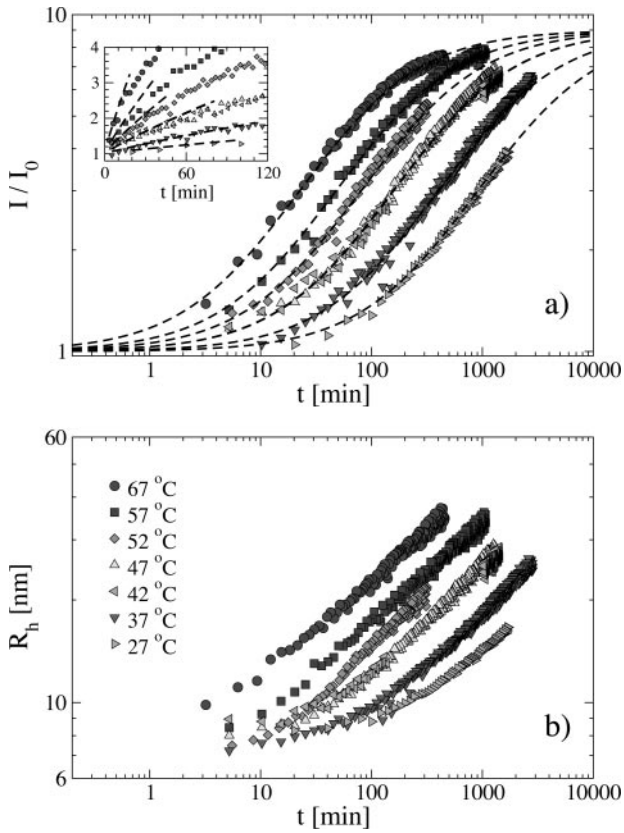

FIG. 2. **Kinetics of aggregation at different temperatures and 185 μM peptide concentration.** *a*, intensities scattered at 90° (I) *versus* time; data are normalized with respect to the initial value I_0. The *dashed lines* are fit to data according to Equation 2. *Inset*: the same quantities of the main figure are plotted with linear axes. *b*, mean hydrodynamic radii *versus* time, calculated by averaging over diffusion coefficient distributions, and assuming the Stokes-Einstein relation.

of 75 (± 15) peptides, and they have a mean hydrodynamic radius of 7 nm. The same results have been obtained at each temperature used: 27, 37, 42, 47, 52, 57, and 67 °C.

We remark that the weight average molecular mass measured by light scattering experiments is defined as $\bar{M}_w = \Sigma_s M_s c_s / c$, where M_s and c_s are, respectively, the molecular mass and the mass concentration of oligomers composed of s peptides. Therefore, a certain amount of single peptides could be present in the solution even if not clearly observable by light scattering measurements, which are more sensitive to large mass objects. The tolerance in the analysis of dynamic light scattering at the initial stage of kinetics allows us to put an upper limit of ~0.4% for the contribution of monomers to scattered intensity. Consequently, in this limit condition, the mass concentration of monomers would be ~30%, and the actual average aggregation number of the oligomeric species would rise up to 110 units.

Early Stages of Kinetics at Different Temperatures—QLS experiments were performed at different temperatures and at the concentration of 185 μM focusing on the early stage of the kinetics. The time dependence of the 90° scattered intensity $I_R(q)$ is shown in Fig. 2*a* for different temperatures. Data were normalized with respect to the initial intensity $I_0(q)$ due to scattering by the initial oligomer distribution. The distribution of hydrodynamic radii at T = 37 °C is shown for selected different times in Fig. 1. For each temperature studied, the distribution remains unimodal over time while its standard deviation and the mean value increase, so that their ratio (which is a measure of the polydispersity) is essentially stationary. The kinetics of the mean hydrodynamic radius is reported in Fig. 2*b* for each temperature.

As shown in the *inset* of Fig. 2*a*, the intensity starts increasing with no lag time. Such growth continues with a temperature-dependent rate and eventually saturates, while the growth of the hydrodynamic radii exhibits no reduction. The saturation of the intensity signal is due to the fact that the scattered intensity is proportional to the average mass of aggregates times the form factor $P(q)$, thus,

$$\frac{I}{I_0} = \frac{\bar{M}_w\, P(q)}{\bar{M}_{w0}\, P_0(q)} \qquad \text{(Eq. 1)}$$

where $\bar{M}_w$ is the weight average molecular mass and the subscript '0' refers to the zero time quantities. During the aggregation process, the average molecular mass increases so that aggregate size becomes larger than the reciprocal scattering vector q = 23 μm^{-1} and the form factor decreases: $P(q) < 1$.

Empirical Fit and Scaling of Kinetics—The intensity growth *versus* time data have a sigmoidal shape on a log-log scale. To describe this behavior, the data were fit to the following empirical expression,

$$\frac{I}{I_0} = 1 + \frac{\left(\frac{t}{\tau_T}\right)^{\beta}}{1 + \frac{1}{\Delta}\left(\frac{t}{\tau_T}\right)^{\beta}} \qquad \text{(Eq. 2)}$$

where β = 0.87, Δ = 8.0, and τ_T = 7.3, 15.5, 26.0, 50.6, 51.2, 129.4, and 293.8 min, respectively, for T = 67, 57, 52, 47, 42, 37, and 27 °C. The exponent β is less than unity, as expected for kinetics with no lag time.

The only fitting parameter depending on temperature is the time constant τ_T, related to an aggregation rate. By plotting the intensity kinetics *versus* the renormalized time t/τ_T, the data collapse on the same master curve (Fig. 3*a*). Remarkably, hydrodynamic radii also scale on a master curve by using the same parameter τ_T (Fig. 3*b*). Therefore, the same aggregation mechanism occurs throughout the temperature range studied.

Suitable Model for the Form Factor—To obtain a basic explanation of this aggregation mechanism, we need to work out a model to fit the experimental kinetic data. An expression for both the growth of the weight average molecular mass $\bar{M}_w$ and for the form factor $P_z(q)$ is required, as is clear from Equation 1. In the present case, we will assume that the shape of aggregates is not critically related to the molecular mass, which is a very reasonable assumption when dealing with polymeric or fibrillar aggregates. Hence, the radius of gyration of aggregates can be written in the following scaling form with respect to the average molecular mass: $R_g = R_{g0}(\bar{M}_w/\bar{M}_{w0})^{1/d}$; where R_{g0} is the initial z-averaged radius of gyration of the oligomers, and d is an effective fractal dimension. Approximating the form factor with the Fisher-Burford expression (53) $P_z(q) = [1 + \frac{2}{3}d^{-1}q^2R_g^2]^{-d/2}$, the time evolution of scattered intensity reads,

$$\frac{I}{I_0} = \frac{\bar{M}_w}{\bar{M}_{w0}} \frac{\left[1 + \frac{2}{3d} q^2 R_{g0}^2 (\bar{M}_w/\bar{M}_{w0})^{2/d}\right]^{-d/2}}{\left[1 + \frac{2}{3d} q^2 R_{g0}^2\right]^{-d/2}} \qquad \text{(Eq. 3)}$$

Our modeling effort is now devoted to finding an expression for the weight average molecular mass, $\bar{M}_w$.

Coagulation Theory—Protein aggregation can be studied in the framework of classic coagulation theory (54), by following an approach that has been widely used for colloids or aerosols (55, 56). The time-dependent aggregation number distribution can be described by the following Smoluchowski equation,

$$\frac{d}{dt} n_s(t) = \frac{1}{2} \sum_{i+j=s} K_{i,j} n_i(t) n_j(t) - n_s(t) \sum_j K_{s,j} n_j(t) \qquad \text{(Eq. 4)}$$

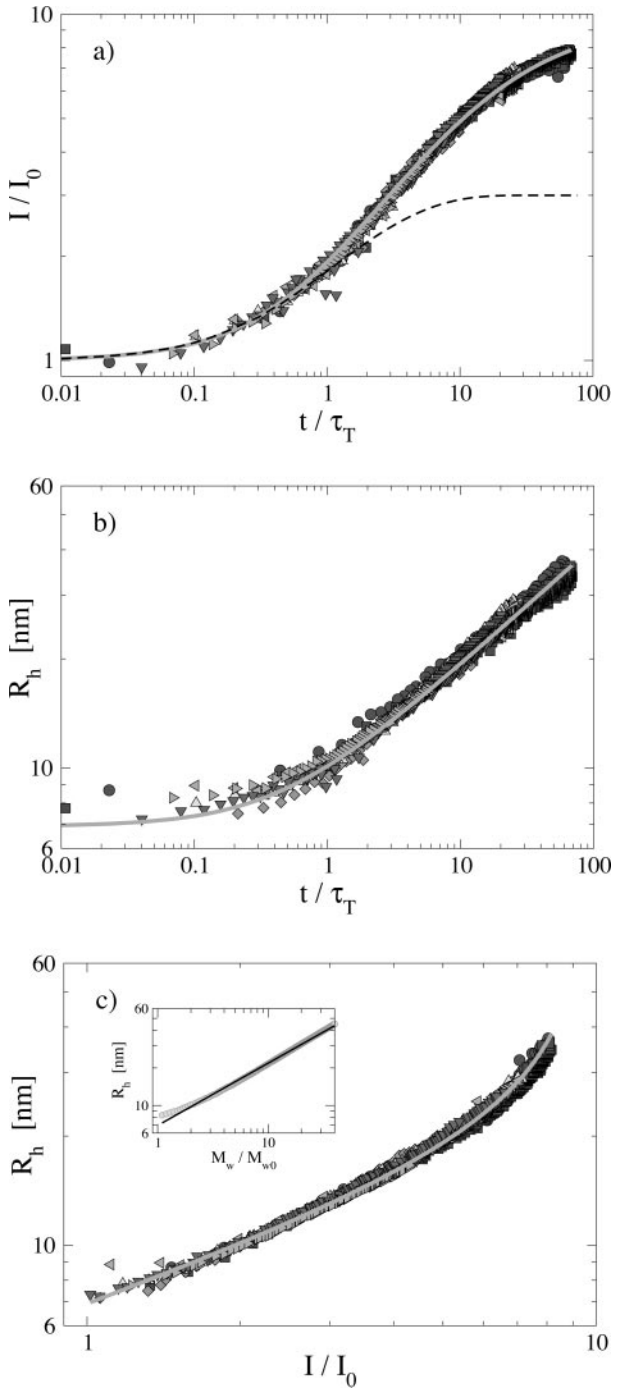

FIG. 3. **Master curve of the kinetics at different temperatures and 185 μM peptide concentration.** *a*, normalized scattering intensity *versus* rescaled time. The *light solid line* is fit to data according to Equations 3 and 7. The *dashed line* represents a numerical solution of Smoluchowski equation (Equation 4) with a kernel allowing monomer only addition (assuming a time independent form factor). *b*, mean hydrodynamic radius *versus* rescaled time. The *light solid line* is fit to data according to Equations 7 and 8. *c*, mean hydrodynamic radius *versus* normalized scattering intensity. The *light solid line* is fit to data according to Equation 3 and 8. *Inset*, hydrodynamic radii *versus* aggregation number; *circles*, expression for flexible rods by Yamakawa and Fujii (64); *solid line*, power law with exponent 0.5.

where n_s is the number concentration of a cluster of s units, and $K_{i,j}$ is the reaction rate of two clusters of i and j units. The two terms in the right-hand side of Equation 4 are, respectively, the production and loss of s-mers by coagulation of two clusters of appropriate size. Here, we are assuming that aggregation is irreversible, so that no fragmentation or evaporation processes occur, and that three-body effects can be neglected. Also, following our discussion above, we do not introduce any nucleation term.

By multiplying Equation 4 by s^k and summing over all s one obtains the time evolution of the moments of the distribution $N_k = \Sigma_s s^k n_s$ (57, 58),

$$\frac{d}{dt}N_k(t) = \frac{1}{2}\sum_{ij} K_{i,j} n_i(t) n_j(t)[(i+j)^k - i^k - j^k] \qquad \text{(Eq. 5)}$$

In particular, the zero and first moments are proportional to the total number and to the mass concentration of clusters, respectively. Note that the conservation of total mass concentration is correctly issued by Equation 5 for $k = 1$:$dN_1/dt = 0$. For our purposes, the most important quantity is the second moment of the distribution N_2, because it is proportional to the weight average molecular mass $\bar{M}_w/\bar{M}_{w0} = N_2/N_1$ and hence to the forward scattered intensity.

Suitable Model for the Intensity Growth—A simple model of fibrillar elongation requires that only monomers can bind to larger clusters. With this prescription, the kernel of the Smoluchowski equation is $K_{i,j} = \gamma/2(\delta_{i,1} + \delta_{j,1})$, where γ is a temperature-dependent parameter, and $\delta_{i,j} = 1$ for $i = j$, and zero otherwise. This kernel is strongly and selectively mass-dependent. The weight average molecular mass $\bar{M}_w$ is given by $\bar{M}_w/\bar{M}_{w0} = 1 + 2M_m/\bar{M}_{w0} \ln[w(x(t))]$, where M_m is the mass of a monomer, and $w(x)$ is the solution of the differential equation, $w'' + w'w^{-1} = 0$. The time-dependent variable $x(t)$ is determined by the initial total number concentration: $x = N_0(0)\gamma t$. In Fig. 3*a*, a numerical solution of this model is reported for the weight average molecular mass by considering the oligomers as the monomeric units, that is $M_m = \bar{M}_{w0}$. It increases up to a saturation value that is too low compared with our experimental data, because this model implies a rapid consumption of available monomers. Note, *a fortiori*, that if we were to consider the time dependence of the form factor the saturation value for I/I_0 would be further lowered from the value shown in the figure. A still lower saturation value would be reached if one considers that the growth is due to addition of single peptides to fibrils starting from an initial distribution of monomer and oligomers, which is $\bar{M}_{w0} = 75M_m$. Therefore, the simpler model where linear aggregates grow by sequential addition of single oligomer units or single peptides can be ruled out by the present experiments.

A suitable model to fit our experimental data should include a more realistic dependence on the mass and the size of aggregates. A simple analytic solution has been worked out theoretically and experimentally for colloidal aggregation (59–62). It requires a kernel that is a homogeneous function of the clusters' mass, or, equivalently, of aggregation numbers, i and j, that is,

$$K_{ai,aj} = a^\lambda K_{i,j} \qquad \text{(Eq. 6)}$$

for any number a. This assumption yields, for $\lambda < 1$ (non-gelling condition),

$$\frac{\bar{M}_w}{\bar{M}_{w0}} = \left(1 + \frac{t}{zt_0}\right)^z, \quad \text{where } z = \frac{1}{1-\lambda} \qquad \text{(Eq. 7)}$$

For $\lambda = 0$, the classic solution with a constant mass-independent kernel is recovered (54). Data shown in Fig. 3*a* are well fit by Equations 3 and 7, with the following fitting parameters: $R_{g0} = 18$ nm, $d = 1.65$, $z = 0.66$ (corresponding to $\lambda = -0.5$), and $t_0 = 0.757\ \tau_T$. The initial R_g is larger than the initial hydrodynamic radius as expected, because it is strongly affected by polydispersity, contrary to the mean hydrodynamic radius that is obtained by averaging over reciprocal values. The value of the fractal dimension d is close

to that found for self-avoiding random coils (63), but in the present case it may be considered as a result of linear elongated flexible aggregates.

Suitable Model for the Hydrodynamic Radius Growth—Along with an increase of the mean weight cluster mass, the increase of aggregate size is mirrored by the growth of the mean hydrodynamic radius. We fit the master curve of hydrodynamic radii (Fig. 3*b*) by using Equation 7 and assuming the following scaling relation between the mean hydrodynamic radius R_h and the weight average molecular mass,

$$R_h^{-1} = R_{h0}^{-1}(\bar{M}_w/\bar{M}_{w0})^{\lambda_h} \qquad \text{(Eq. 8)}$$

where R_{h0} = 6.9 nm and $\lambda_h = -0.5$. Also, Equations 3 and 8 have been used to fit data for the hydrodynamic radius *versus* intensity (Fig. 3*c*), with the same parameters obtained in the two previous fitting procedures reported in Fig. 3 (*a* and *b*): R_{h0} = 6.9 nm, $\lambda_h = -0.5$, and R_{g0} = 18 nm, d = 1.65. Unlike the radius of gyration, the hydrodynamic radius is not determined solely by the shape and size of an object but also by its diffusion properties. In fact, the exponents used for the scaling relations of hydrodynamic and gyration radii are, respectively, $-\lambda_h = 0.5$ and $1/d = 0.6$, analogously to what has been found in the case of self-avoiding random polymers (63). We also note that the growth of these polymeric aggregates occurs in a very dilute regime due to the small length of the chains and the low peptide concentration, ruling out the effect of interparticle interaction on the measured hydrodynamic properties. A power law, as in Equation 8, with exponent 0.5, is a very good approximation for the case of flexible rods, when the mean aggregation number $\hat{s}$ is relatively small, as in the present experiments. In fact, we are considering that the building unit of a fibril is not the single Aβ peptide, but the "average" oligomer observed at the onset of kinetics: $\hat{s} = \bar{M}_w/\bar{M}_{w0} < 30$. To easily visualize the goodness of this approximation, in the *inset* of Fig. 3*c* we plot indeed the expression derived by Yamakawa and Fujii (64) for flexible rods with a persistence length equivalent to the diameter of the rod d_0 = 14 nm, together with a power law $R_h = d_0/2\hat{s}^{0.5}$. From the estimated persistence length we could calculate the contour length of these linear flexible aggregates. For example, when the hydrodynamic radius is 35 nm, the contour length would be 350 nm.

Structure of the Kernel—A very striking point of the present results is that the exponent λ_h is equivalent to the exponent λ of the coagulation kernel in the Smoluchowski equation (Equation 4). From coagulation theory (54), one can write a quite general expression for the kernel $K_{i,j}$, depending upon both the diffusion coefficients of clusters made of i and j units, D_i and D_j, and the correspondent spheres of influence of such clusters, with radii R_i and R_j, which are related to the size of their binding sites,

$$K_{i,j} = 4\pi(D_i + D_j)\frac{1}{2}(R_i + R_j)g_{ij}e^{-\Delta G/k_BT} \qquad \text{(Eq. 9)}$$

where ΔG is the size-independent free energy change associated with coagulation of two clusters and g_{ij} is a geometric factor related to coagulation probability. Expressions for the hydrodynamic radius (65) and for the sticking probability (66) of rigid fibrils have been reported and used to numerically integrate the Smoluchowski equation for the case of amyloid formation (36, 67, 68). In the present experiments, the kernel homogeneity and the equivalence between the mentioned exponents obtained from data analysis ($\lambda = \lambda_h = -0.5$) allow us to assign all the mass dependence to the hydrodynamic radii. In fact, by using the Stokes-Einstein relation and an expression equivalent to Equation 8 for any aggregation number i, the Equation 9 fulfills Equation 6 as follows.

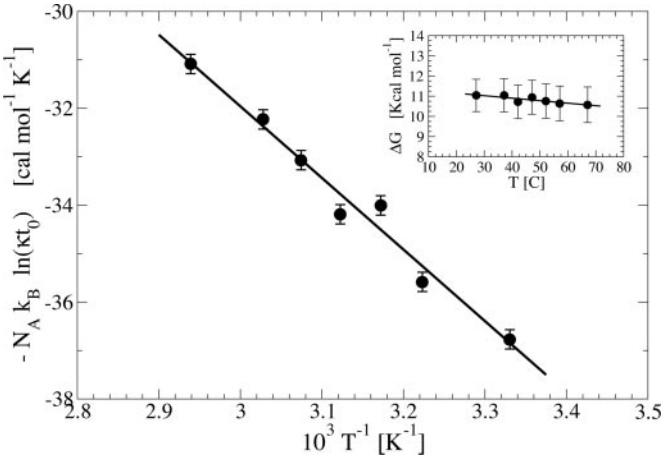

FIG. 4. **Arrhenius plot for the 185 μM peptide concentration.** The *solid line* is a linear fit to data. *Inset*, free energy barrier *versus* temperature.

$$K_{i,j} = \frac{4k_BT}{3\eta}g\frac{i^{-0.5} + j^{-0.5}}{2}e^{-\Delta G/k_BT} \qquad \text{(Eq. 10)}$$

The parameter $g = g_{ij}\frac{1}{2}(R_i + R_j)/R_{h0}$ can be reasonably taken equal to one, if we put $g_{ij} = 1$ and consider that the sphere of influence of each cluster is of the order of R_{h0}. We see that the temperature dependence of the kernel is then separated from the mass dependence. This fact explains the scaling of aggregation kinetics in Fig. 3, which have an identical evolution apart from a characteristic time $t_0^{-1} = \kappa\exp(-\Delta G/k_BT)$, where $\kappa = 4k_BT/3\eta c/\bar{M}_{w0}$.

Temperature Dependence of the Aggregation Rate—The free energy barrier associated with the aggregation process can be estimated from the temperature dependence of the aggregation rate. In Fig. 4, the quantity $-N_Ak_B\ln(\kappa t_0)$ (where N_A is Avogadro's number) is plotted *versus* the reciprocal temperature (Arrhenius plot). Data are well fit by a straight line,

$$-N_Ak_B\ln(\kappa t_0) = \Delta S - \frac{\Delta H}{T} \qquad \text{(Eq. 11)}$$

where ΔS and ΔH are, respectively, the entropy and enthalpy costs associated with coagulation. From the fit, we obtain ΔS = 12 ± 2 cal mol^{-1}K^{-1} and ΔH = 14.8 ± 0.3 kcal mol^{-1}, with a corresponding average free energy of ΔG = 11 ± 1 kcal mol^{-1} (value at 37 °C). The error associated with ΔH is mainly due to the experimental error on the characteristic times t_0, which is on the order of 2%. On the other hand, the error in the entropic term ΔS, and consequently in the free energy, is affected also by the intrinsic indetermination in the quantity g that appears in Equation 10. If we assume an error in g of 100%, the error in ΔS is on the order of N_Ak_B.

Early Stages of Kinetics at Different Concentrations—To check the validity of the proposed kinetic model, we report QLS experiments on the early stage of the kinetics performed at 37 °C and at two additional concentrations: 92 and 277 μM. Kinetics of intensity and hydrodynamic radius are reported in Fig. 5, together with the already shown kinetics at 185 μM concentration. Times are scaled according to the parameter $\tau_T(c)$, which depends on both temperature and concentration as $\tau_T(c) = \tau_T\, c/c_{185}$, where τ_T is the parameter already reported for the concentration of the main set of experiments (185 μM), and c/c_{185} is the ratio between the concentration of each sample and the concentration of 185 μM. At the higher concentration, data can be scaled in agreement with the proposed model, whereas at the lower concentration the model seems to fail.

Aggregation Kinetics from Oligomers to Large Size Tangles—The kinetics of aggregation has been monitored up to the for-

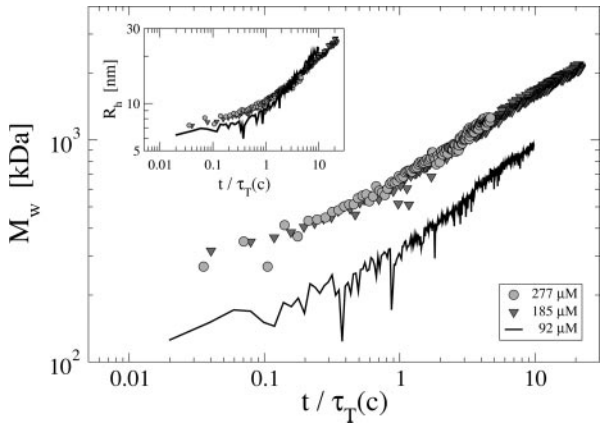

FIG. 5. **Kinetics of aggregation at 37 °C and at different peptide concentrations.** Apparent weight average molecular mass ($\bar{M}_w$) *versus* time. Times are scaled according to the parameter $\tau_T(c)$, which depends on both temperature and concentration. *Inset*: Mean hydrodynamic radius *versus* time, calculated by averaging over diffusion coefficient distributions and assuming the Stokes-Einstein relation.

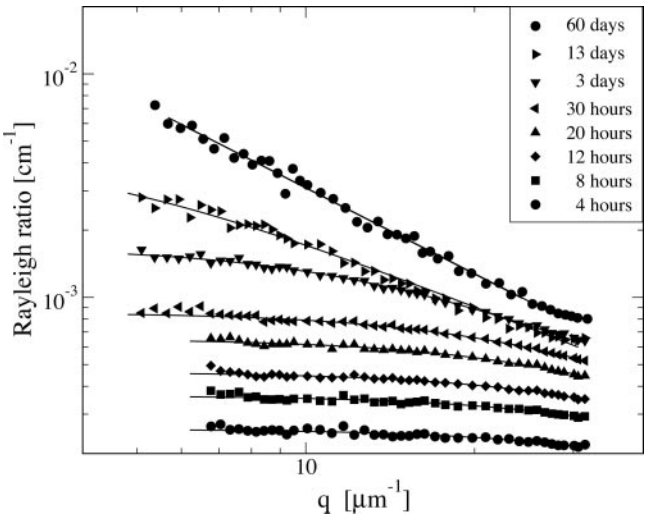

FIG. 6. **Time evolution of the Rayleigh ratio of Aβ fibrils and aggregates at 37 °C and 185 μM peptide concentration.** Solid lines are fit to data by using the Guinier expression (from 4 to 30 h), the Fisher-Burford expression (3 and 13 days), and a power law (60 days).

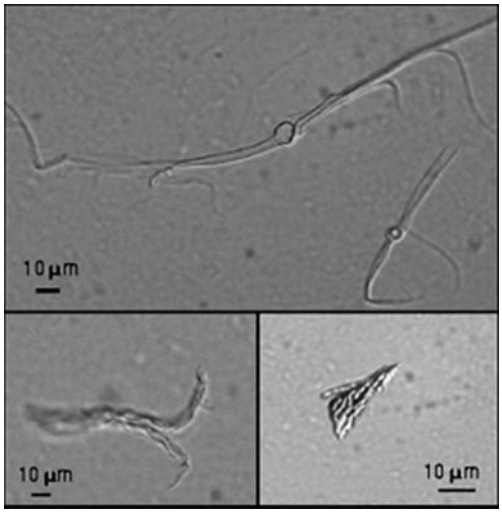

FIG. 7. **Images of Aβ(1–40) clusters after two months of incubation at 37 °C and 185 μM peptide concentration.** Fibril tangles of different shape can be observed.

mation of large size clusters of fibrils, which are clearly observable after 2 months (Figs. 6 and 7). By measuring the scattered intensity at different angles, which is at different scattering vectors, we have obtained the z-averaged form factor $P_z(q)$, which can be used to estimate the z-averaged radius of gyration R_g. In the early stage (first day), when aggregate size is still smaller than 100 nanometers, only a rough estimate of R_g was possible via the Guinier expression: $P_z(q) = [1 + \frac{1}{3}q^2R_g^2]^{-1}$. During the next weeks, the clusters size slowly increased up to tens of microns. The form factor of such clusters can be modeled by using the mentioned Fisher-Burford expression (53), with an effective fractal dimension d close to one. The form factor measured after two months of aging reveals a clear power law behavior ($P_z(q) \sim q^{-d}$) and a fractal dimension $d = 1.3$, which mirrors the structure of clusters of fibers, as clearly seen by optical microscopy measurements (see Fig. 7). However, the aggregates observed at these late stages are not directly related to the mechanism revealed by the early stage experiments, and their formation and morphological variety are not addressed by the present work.

DISCUSSION

Aggregation kinetics of Aβ(1–40) have been monitored by light scattering techniques at pH 3.1 and at different temperatures: 27, 37, 42, 47, 52, 57, and 67 °C. At this pH, the kinetics of Aβ(1–40) self-assembly are highly reproducible, mainly due to the lack of a significant amount of spurious nucleation seeds.

Onset of Kinetics: Large Oligomers—After dissolution of peptides in aqueous solution, QLS measurements reveal the presence of oligomeric species with a unimodal distribution of hydrodynamic radii peaked at the value of 7 nm (Fig. 1*a*). The average molecular mass is 330 ± 60 kDa, corresponding to an assembly of 75 ± 15 Aβ(1–40). As remarked in the previous section, the presence of monomeric Aβ is not excluded by the presence of larger size oligomers and by the high average molecular mass. These findings are in reasonable agreement with the results of Huang *et al.* (28) who have estimated, under analogous conditions, a molecular mass of Aβ(1–40) oligomers in the range between 0.5 and 1.4 MDa and a mean diameter of 15 nm. At more acid conditions (pH 2), Lomakin *et al.* (35–37, 39) have found that Aβ(1–40) are assembled into spherocylindrical micelles of mean hydrodynamic diameter of 14 nm and made up of about 25 peptides . Such low-pH oligomers are considerably larger than those involved in Aβ fibrillogenesis under physiological conditions (9, 25, 28), as well as from typical oligomeric intermediates found in other protein aggregation processes (18, 69–71).

Early Stage of Kinetics: One Single, Non-cooperative Process—To unravel the mechanism of protofibril formation starting from oligomers, we focused on the early stage of aggregation kinetics, by measuring essentially two quantities: light scattered intensity, which is closely related to the average mass of aggregates, and hydrodynamic radius, which is related to the size and the diffusion properties (and hence the shape) of aggregates (Fig. 2).

Kinetics at different temperatures (in the range 27–67 °C) can be scaled on a single master curve by renormalizing the timescale, that is, by using only one parameter t_0 related to the reciprocal aggregation rate (Fig. 3). Also, each set of kinetic data shows no lag time, because the growth of both intensities and hydrodynamic radii have a non-zero derivative at time $t = 0$. Thus, present experiments show that at pH 3.1, protofibril formation occurs via a single elongation process, which operates at different temperatures, with no observable nucleation step.

Of course, the time resolution of our experiments does not allow us to completely rule out the occurrence of nucleation

within the first minute after sample preparation. However, measurements at the onset of the kinetics at each temperature show the same distribution of oligomers with large molecular mass and size. Thus, nuclei formation, if any, has gone to completion within tens or hundreds of seconds with a very high rate. We can state that, under the present conditions, nucleation is not a rate-limiting step for amyloid formation.

Arrhenius Plot: One Single Barrier—The time-scale parameter t_0 is linearly correlated with reciprocal temperature (on a semilogarithmic scale) (Fig. 4). This implies that aggregation is controlled by one single free energy barrier, associated with the activation of the intermediate state in the coagulation process. We measured the enthalpic and entropic costs associated with this process to be $\Delta H = 14.8 \pm 0.3$ kcal mol^{-1} and $\Delta S = 12 \pm 2$ cal mol^{-1}K^{-1}, with a corresponding average free energy at 37 °C of $\Delta G = 11 \pm 1$ kcal mol^{-1}.

These results are consistent with the work of Kusumoto *et al.* (37), which is the only comparable report in the literature. They have estimated the following values for the elongation process of Aβ(1–40) at pH 2: $\Delta H = 23$ kcal mol^{-1}, $\Delta S = 53$ cal mol^{-1}K^{-1}, and $\Delta G_{T = 300°K} = 7$ kcal mol^{-1}. As remarked by these authors, such a value of activation free energy is reminiscent of those expected for conformational changes of a protein or a peptide. At physiological pH, low molecular weight oligomers of Aβ(1–40) have been found to undergo a conformational change, with a subtle balance of α and β structures, to bind to amyloid fibrils (72, 73). The estimated activation free energies are a few kcal mol^{-1}. In the present case, we can argue that along with a conformational change related to the single peptide, a local reorganization of each aggregate may be involved to incorporate large molecular weight oligomers, analogously to what is observed in rod-like micelles (74, 75).

Modeling Coagulation: Diffusion and Reaction of Protofibrils and Exclusion of Monomer-only Addition—Scaled kinetic data have been analyzed in terms of linear colloidal aggregation (33, 76). We have found that the growth of cluster mass and size can be described by a Smoluchowski equation with a homogeneous kernel associated with the coagulation rate (Equations 4 and 9). These results have been achieved by simultaneous fitting of intensity and hydrodynamic radius growth with time at different temperatures (Fig. 3). In particular, it has been found that the exponent λ_h, used to model the dependence of the mean hydrodynamic radius R_h on the average molecular mass (Equation 8) is equal to the exponent λ, which indicates the rank of homogeneity of the kernel (Equation 6). This implies that the coagulation rate has a mass dependence given entirely by the hydrodynamic radii of aggregates, *i.e.* by their diffusional properties, and that the free energy of activation related to cluster coalescence does not depend on their mass. Also, the typical model of fiber growth by monomer-only addition is straightforwardly ruled out. Thus, the elongation model seems to be different from that observed at pH 7.4, where elongation occurs by addition of single intermediate units (46, 47, 67). A reasonable explanation for this different behavior is that the distributions of oligomeric species initially present in solution are quite different in the two cases, because, as discussed above, they depend on pH and other thermodynamic quantities (28, 77).

Model Validity and Generality: Dependence on the Initial Conditions—In addition to the main set of kinetics at different temperatures and at the concentration of 185 μM, we performed two experiments at 37 °C at a lower (92 μM) and a higher concentration (277 μM) (Fig. 5). Although this is a very preliminary report of an ongoing work, it allows us to check the validity of our kinetic model. Kinetic data can be scaled accordingly to the proposed model in the case of the higher concentration, whereas at the lower concentration the model fails. This is reasonably due to the different initial conditions that are observed at low concentration, where both the mean hydrodynamic radius and the average molecular mass are lower than the other two cases. Interestingly, this is in close agreement with the results of Lomakin *et al.* (35), who have found, for a solution of Aβ(1–40) at pH 2, a critical micellar concentration of about 100 μM. Thus, our model seems to be easily extendable to a high concentration range where the solution exhibits an analogous initial distribution of oligomers.

Late Stage of Kinetics: Clusters of Fibrils—The aggregation process has been monitored for several weeks, until amyloid fibrils assemble into large size clusters (hundreds of microns). Such clusters have an apparent fractal dimension of 1.3 on the submicron scale (Fig. 6), because they originate from the aggregation of already formed elongated fibrils (see Fig. 7). Their aggregation mechanism is of course not equivalent to that revealed by our early stage kinetic experiments.

Concluding Remarks—The kinetics of amyloid fibrillation are important to understand the mechanism of amyloid self-assembly and to eventually design molecular inhibitors. A complex panorama of different macromolecular structures (protofibrils, filaments, and fibers) is usually present both in the case of the Alzheimer amyloid β-protein and in other amyloidogenic proteins (78–80). Although our experiments do not directly investigate the physiology of the pathologic assembly, they address Aβ(1–40) self-organization at the molecular level and thus contribute to understand a few basic features of the molecular interactions and mechanisms that drive amyloid fibrillogenesis. Under the particular condition studied (pH 3.1 and high concentrations), flexible protofibrils are formed from a solution containing large molecular weight oligomers by diffusion and coagulation of aggregates of different size, through an activation free energy of about 11 kcal mol^{-1}. The specific structure of such oligomers and the nature of the activation barrier, which is still not established, is the subject of ongoing work. The existence of a non-cooperative elongation process casts amyloid formation into an anti-pathogenic process that sequesters toxic oligomeric products. Apart from this interesting suggestion, the present work puts the important mechanism of amyloid formation on firmer basic physical grounds.

Acknowledgments—We thank D. Giacomazza, R. Noto, J. Newman, F. Librizzi, G. Tiana, M. Di Carlo, D. Romancino, P. A. Temussi, and S. Hansen for relevant discussions and collaborations. We are grateful to J. Newman for critical reading of the manuscript.

REFERENCES

1. Selkoe, D. J. (1999) *Nature* **399,** A23–A31
2. Kelly, J. W. (1996) *Curr. Opin. Struct. Biol.* **6,** 11–17
3. Lansbury, P. T., Jr. (1999) *Proc. Natl. Acad. Sci. U. S. A.* **96,** 3342–3344
4. Chiti, F., Webster, P., Taddei, N., Clark, A., Stefani, M., Ramponi, G., and Dobson, C. M. (2002) *Proc. Natl. Acad. Sci. U. S. A.* **96,** 3590–3594
5. Hardy, J., and Selkoe, D. J. (2002) *Science* **297,** 353–356
6. Selkoe, D. J., and Podlisny, M. B. (2002) *Annu. Rev. Genomics Human Genetics* **3,** 67–99
7. Terry, R. D., Masliah, E., Salmon, D. P., Butters, N., DeTeresa, R., Hill, R., Hansen, L. A., and Katzman, R. (1991) *Ann. Neurol.* **30,** 572–580
8. Selkoe, D. J. (2002) *Science* **298,** 789–791
9. Lambert, M. P., Barlow, A. K., Chromy, B. A., Edwards, C., Freed, R., Liosatos, M., Morgan, T. E., Rozovsky, I., Trommer, B., Viola, K. L., Wals, P., Zhang, C., Finch, C. E., Krafft, G. A., and Klein, W. L. (1998) *Proc. Natl. Acad. Sci. U. S. A.* **95,** 6448–6453
10. Hoshi, M., Sato, M., Matsumoto, S., Noguchi, A., Yasutake, K., Yoshida, N., and Sato, K. (2003) *Proc. Natl. Acad. Sci. U. S. A.* **100,** 6370–6375
11. Kuo, Y. M., Emmerling, M. R., Vigo-Pelfrey, C., Kasunic, T. C., Kirkpatrick, J. B., Murdoch, G. H., Ball, M. J., and Roher, A. E. (1996) *J. Biol. Chem.* **271,** 4077–4081
12. Roher, A. E., Chaney, M. O., Kuo, Y. M., Webster, S. D., Stine, W. B., Haverkamp, L. H., Woods, A. S., Cotter, R. J., Tuohy, J. M., Krafft, G. A., Bonnell, B. S., and Emmerling, M. R. (1996) *J. Biol. Chem.* **271,** 20631–20635
13. Walsh, D. M., Klyubin, I., Fadeeva, J. V., Cullen, W. K., Anwyl, R., Wolfe, M. S., Rowan, M. J., and Selkoe, D. J. (2002) *Nature* **416,** 535–539
14. McLaurin, J., and Chakrabartty, A. (1996) *J. Biol. Chem.* **271,** 26482–26489
15. Yip, C. M., and McLaurin, J. (2001) *Biophys. J.* **80,** 1359–1371

16. Kremer, J. J., Pallitto, M. M., Sklansky, D. J., and Murphy, R. M. (2001) *Biochemistry* **39,** 10309–10318
17. Lashuel, H. A., Hartley, D., Petre, B. M., Walz, T., and Lansbury, P. T. J. (2002) *Nature* **418,** 291–291
18. Stefani, M., and Dobson, C. M. (2003) *J. Mol. Med.* **81,** 678–699
19. Kirkitadze, M. D., Bitan, G., and Teplow, D. B. (2001) *J. Neurosci. Res.* **69,** 567–577
20. Klein, W. L., Stine, W. B. J., and Teplow, D. B. (2004) *Neurobiol. Aging* **25,** 569–580
21. Blackley, H. K. L., Patel, N., Davies, M. C., Roberts, C. J., Tendler, S. J. B., Wilkinson, M. J., and Williams, P. M. (1999) *Exp. Neurol.* **158,** 437–443
22. Blackley, H. K. L., Sanders, G. H. W., Davies, M. C., Roberts, C. J., Tendler, S. J. B., and Wilkinson, M. J. (2000) *J. Mol. Biol.* **298,** 833–840
23. Westlind-Danielsson, A., and Arnerup, G. (2001) *Biochemistry* **40,** 14736–14743
24. Walsh, D. M., Lomakin, A., Benedek, G. B., Condron, M. M., and Teplow, D. B. (1997) *J. Biol. Chem.* **272,** 22364–22372
25. Walsh, D. M., Hartley, D. M., Kusumoto, Y., Fezoui, Y., Condron, M. M., Lomakin, A., Benedek, G. B., Selkoe, D. J., and Teplow, D. B. (1999) *J. Biol. Chem.* **274,** 25945–25952
26. Bitan, G., Lomakin, A., and Teplow, D. B. (2001) *J. Biol. Chem.* **276,** 35176–35284
27. Bitan, G., Kirkitadze, M. D., Lomakin, A., Vollers, S. S., Benedek, G. B., and Teplow, D. B. (2003) *Proc. Natl. Acad. Sci. U. S. A.* **100,** 330–335
28. Huang, T. H. J., Yang, D. S., Plaskos, N. P., Go, S., Yip, C. M., Fraser, P. E., and Chakrabartty, A. (2000) *J. Mol. Biol.* **297,** 73–87
29. Gorman, P. M., Yip, C. M., Fraser, P. E., and Chakrabartty, A. (2003) *J. Mol. Biol.* **325,** 743–757
30. Stine, W. B., Dahlgren, K. N., Krafft, G. A., and LaDu, M. J. (2003) *J. Biol. Chem.* **278,** 11612–11622
31. Rochet, J. C., and Lansbury, P. T. J. (2000) *Curr. Opin. Struct. Biol.* **10,** 60–68
32. Relini, A., Torrassa, S., Rolandi, R., Gliozzi, A., Rosano, C., Canale, C., Bolognesi, M., Plakoutsi, G., Bucciantini, M., Chiti, F., and Stefani, M. (2004) *J. Mol. Biol.* **338,** 943–957
33. Xu, S., Bevis, B., and Arnsdorf, M. F. (2001) *Biophys. J.* **81,** 446–454
34. Kheterpal, I., Lashuel, H. A., Hartley, D. M., Walz, T., Lansbury, P. T., Jr., and Wetzel, R. (2003) *Biochemistry* **42,** 14092–14098
35. Lomakin, A., Chung, D. S., Benedek, G. B., Kirschner, D. A., and Teplow, D. B. (1996) *Proc. Natl. Acad. Sci. U. S. A.* **93,** 1125–1129
36. Lomakin, A., Teplow, D. B., Kirschner, D. A., and Benedek, G. B. (1997) *Proc. Natl. Acad. Sci. U. S. A.* **94,** 7942–7947
37. Kusumoto, Y., Lomakin, A., Teplow, D. B., and Benedek, G. B. (1998) *Proc. Natl. Acad. Sci. U. S. A.* **95,** 12277–12282
38. Huang, T. H. J., Yang, D. S., Fraser, P. E., and Chakrabartty, A. (2000) *J. Biol. Chem.* **275,** 36436–36440
39. Yong, W., Lomakin, A., Kirkitadze, M. D., Teplow, D. B., Chen, S.-H., and Benedek, G. B. (2002) *Proc. Natl. Acad. Sci. U. S. A.* **99,** 150–154
40. Ban, T., Hoshino, M., Takahashi, S., Hamada, D., Hasegawa, K., Naiki, H., and Goto, Y. (2004) *J. Mol. Biol.* **344,** 757–767
41. Oosawa, F., and Asakura, S. (1975) *Thermodynamics of the Polymerization of Proteins*, Academic Press, London
42. Flyvbjerg, H., Jobs, E., and Leibler, S. (1996) *Proc. Natl. Acad. Sci. U. S. A.* **93,** 5975–5979
43. Jarrett, J. T., Berger, E. P., and Lansbury, P. T. J. (1993) *Biochemistry* **32,** 4693–4697
44. Harper, J. D., and Lansbury, P. T. J. (1997) *Annu. Rev. Biochem.* **66,** 385–407
45. Naiki, H., and Geiyo, F. (1999) *Methods Enzymol.* **309,** 305–319
46. Murphy, R. M., and Pallitto, M. M. (2000) *J. Struct. Biol.* **130,** 109–122
47. Pallitto, M. M., and Murphy, R. M. (2001) *Biophys. J.* **81,** 1805–1822
48. Shen, C. L., Fitzgerald, M. C., and Murphy, R. M. (1994) *Biophys. J.* **67,** 1238–1246
49. Crescenzi, O., Tomaselli, S., Guerrini, R., Salvadori, S., D'Ursi, A. M., Temussi, P. A., and Picone, D. (2002) *Eur. J. Biochem.* **269,** 5642–5648
50. Edelhoch, H. (1967) *Biochemistry* **6,** 1948–1954
51. Stepanek, P. (1993) in *Dynamic Light Scattering: The Method and Some Applications* (Brown, W., ed) pp. 177–241, Clarendon Press, Oxford
52. Berne, B. J., and Pecora, R. (1976) *Dynamic Light Scattering*, Wiley-Interscience, New York
53. Nicolai, T., Durand, D., and Gimel, J.-C. (1993) in *Light Scattering: Principles and Development* (Brown, W., ed) pp. 201–231, Clarendon Press, Oxford
54. Chandrasekhar, S. (1943) *Rev. Mod. Phys.* **15,** 1–89
55. Family, F., and Landau, D. P. (1984) *Kinetics of Aggregation and Gelation*, North-Holland, Amsterdam
56. Weitz, D. A., Huang, J. S., Lin, M. Y., and Sung, J. (1984) *Phys. Rev. Lett.* **53,** 1657–1660
57. Taylor, T. W., and Sorensen, C. M. (1987) *Phys. Rev. A* **36,** 5415–5419
58. Krapivsky, P. L., and Redner, S. (1996) *Phys. Rev. E* **54,** 3553–3561
59. Vicsek, T., and Family, F. (1984) *Phys. Rev. Lett.* **52,** 1669–1672
60. van Dongen, P. G. J., and Ernst, M. H. (1985) *Phys. Rev. Lett.* **54,** 1396–1399
61. Weitz, D. A., and Lin, M. Y. (1986) *Phys. Rev. Lett.* **57,** 2037–2040
62. Olivier, B. J., and Sorensen, C. M. (1990) *Phys. Rev. A* **41,** 2093–2100
63. de Gennes, P.-G. (1979) *Scaling Concepts in Polymer Physics*, pp. 38–43, Cornell University Press, Ithaca and London
64. Yamakawa, H., and Fujii, M. (1973) *Macromolecules* **6,** 407–415
65. Tirado, M. M., Lopez Martinez, C., and Garcia de la Torre, J. (1984) *J. Chem. Phys.* **81,** 2047–2052
66. Hill, T. L. (1983) *Biophys. J.* **44,** 285–288
67. Tomski, S., and Murphy, R. M. (1992) *Arch. Biochem. Biophys.* **294,** 630–638
68. Thunecke, M., Lobbia, A., Kosciessa, U., Dyrks, T., Oakley, A. E., Turner, J., Saenger, W., and Georgalis, Y. (1998) *J. Peptide Res.* **52,** 509–517
69. Bauer, R., Carrotta, R., Rischel, C., and Ogendal, L. (2000) *Biophys. J.* **79,** 1030–1038
70. Carrotta, R., Bauer, R., Waninge, R., and Rischel, C. (2001) *Prot. Sci.* **10,** 1312–1318
71. Bulone, D., Martorana, M., and San Biagio, P. L. (2001) *Biophys. Chem.* **91,** 61–69
72. Kirkitadze, M. D., Condron, M. M., and Teplow, D. B. (2001) *J. Mol. Biol.* **312,** 1103–1119
73. Fezoui, Y., and Teplow, D. B. (2002) *J. Biol. Chem.* **277,** 36948–36954
74. Porte, G., and Appell, J. (1981) *J. Phys. Chem.* **85,** 2511–2519
75. Magid, L. (1993) in *Dynamic Light Scattering: The Method and Some Applications* (Brown, W., ed) pp. 554–593, Clarendon Press, Oxford
76. Modler, A. J., Gast, K., Lutsch, G., and Damaschun, G. (2003) *J. Mol. Biol.* **325,** 135–148
77. Klug, G. M. J. A., Losic, D., Subasinghe, S. S., Aguilar, M.-I., Martin, L. L., and Small, D. H. (2003) *Eur. J. Biochem.* **270,** 4282–4293
78. Harper, J. D., Wong, S. S., Lieber, C. M., and Lansbury, P. T. J. (1999) *Biochemistry* **38,** 8972–8980
79. Nichols, M. R., Moss, M. A., Reed, D. K., Lin, W. L., Mukhopadhyay, R., Hoh, J. H., and Rosenberry, T. L. (2002) *Biochemistry* **41,** 6115–6127
80. Khurana, R., Ionescu-Zanetti, C., Pope, M., Li, J., Nielson, L., Ramirez-Alvarado, M., Regan, L., Fink, A. L., and Carter, S. A. (2003) *Biophys. J.* **85,** 1135–1144

Protofibril Formation of Amyloid β-Protein at Low pH via a Non-cooperative Elongation Mechanism

Rita Carrotta, Mauro Manno, Donatella Bulone, Vincenzo Martorana and Pier Luigi San Biagio

J. Biol. Chem. 2005, 280:30001-30008.
doi: 10.1074/jbc.M500052200 originally published online June 28, 2005
